Detecting vacuum birefringence with X-ray free electron lasers and high-power optical lasers

A feasibility study

Hans-Peter Schlenvoigt[1], Tom Heinzl[2], Ulrich Schramm[1,3], Thomas E. Cowan[1,3], Roland Sauerbrey[1,3]

[1] *Helmholtz-Zentrum Dresden – Rossendorf, Institute of Radiation Physics*
[2] *School of Computing and Mathematics, Plymouth University*
[3] *Technische Universität Dresden*

November 2, 2015

HZDR

DRESDEN concept

HELMHOLTZ ZENTRUM DRESDEN ROSSENDORF

Light-by-light scattering

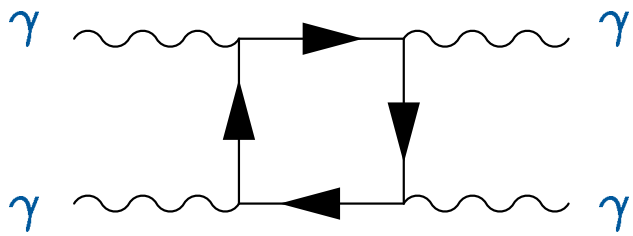

Figure 1 – Light-by-light scattering to lowest order in QED.

- all 4 photons real: Vacuum birefringence, not yet observed
- all 4 photons virtual:
  - subdiagram in $g-2$, ultra-well-tested to 0.24 ppb [1], LBL $\sim 10^{-5}$
  - subdiagram in Lamb shift, well-tested, led to "Proton radius puzzle" [2]
- Delbrück scattering [3]: 2 real photons plus nucleus Coulomb field, difficult to isolate in experiments

Estimated ellipticity for all-laser VB

$$
\begin{aligned}
|\delta|^2 &\propto \alpha^2 \left(\frac{d}{\lambda}\right)^2 \left(\frac{E}{E_S}\right)^4 \\
&\approx \left(\frac{1}{137}\right)^2 \cdot \left(\frac{10\,\mu\mathrm{m}}{1\,\text{Å}}\right)^2 \cdot \left(10^{-4}\right)^4 \\
&\sim 10^{-11} \text{ ([4], this proposal)}
\end{aligned}
\tag{1}
$$

DRESDEN concept

HZDR

Estimated ellipticity for all-laser VB

$$
\begin{aligned}
|\delta|^2 &\propto \alpha^2 \left(\frac{d}{\lambda}\right)^2 \left(\frac{E}{E_S}\right)^4 \\
&\approx \left(\frac{1}{137}\right)^2 \cdot \left(\frac{10\,\mu\mathrm{m}}{1\,\text{Å}}\right)^2 \cdot \left(10^{-4}\right)^4 \\
&\sim 10^{-11} \text{ ([4], this proposal)} \\
&\gg \left(\frac{1}{137}\right)^2 \cdot \left(10^5 \times \frac{1\,\mathrm{m}}{1\,\mu\mathrm{m}}\right)^2 \cdot \left(10^{-9}\right)^4 \\
&\sim 10^{-19} \text{ (optical probe in magnet)}
\end{aligned}
\tag{1}
$$

Basic geometry

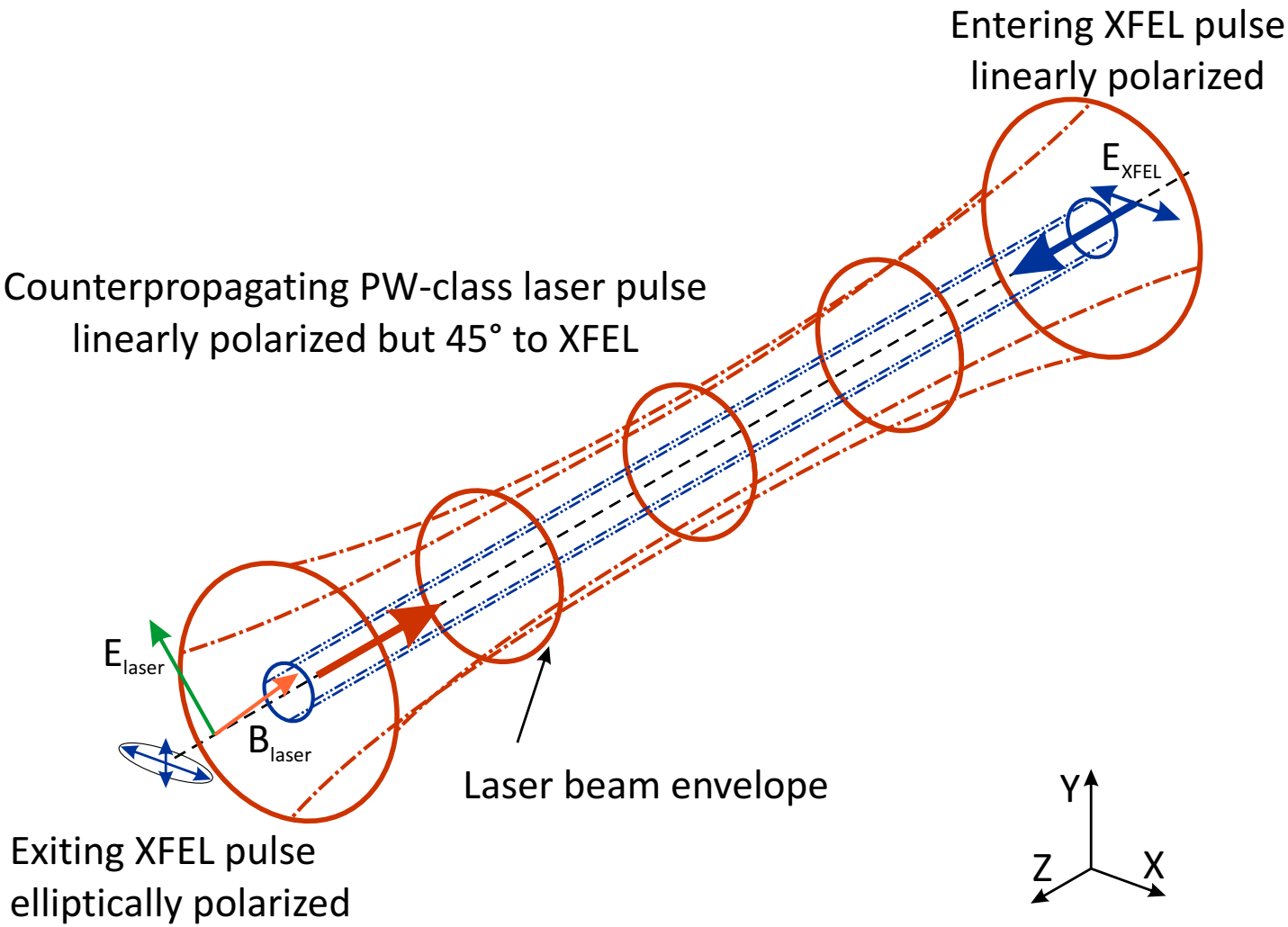

Basic geometry

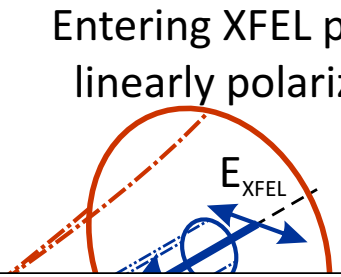

Disclaimer

Strict forward scattering $\mathbf{k} \equiv \mathbf{k}'$ and only polarization-flip $\varepsilon \cdot \varepsilon' = 0$ (as discussed by Heinzl et. al. , Opt.Comm., 2006 [4]). Recent work by F. Karbstein et. al. [5, `http://arxiv.org/abs/1507.01084v1`, accepted in Phys. Rev. D; see also two talks later] includes small scattering angles.

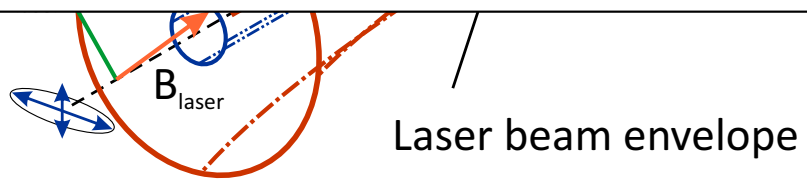

Exiting XFEL pulse
elliptically polarized

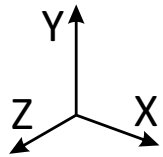

Single photon phase shift

$$\Delta\phi = 2\pi \frac{d}{\lambda_X} \Delta\eta = \frac{4\alpha}{15} \frac{d}{\lambda_X} \frac{l_L}{l_S} \tag{2}$$

Single photon phase shift

$$\Delta\phi = 2\pi \frac{d}{\lambda_X} \Delta\eta = \frac{4\alpha}{15} \frac{d}{\lambda_X} \frac{l_L}{l_S} \tag{2}$$

$$\phi(t) = \frac{4\alpha}{15} \frac{1}{l_S \lambda_X} \int_{-\infty}^{t} l_L(X, Y, c_0(t' - T), t') \underbrace{c_0 \, \mathrm{d}t'}_{\mathrm{d}z} \tag{3}$$

Single photon phase shift

$$\Delta\phi = 2\pi \frac{d}{\lambda_X} \Delta\eta = \frac{4\alpha}{15} \frac{d}{\lambda_X} \frac{I_L}{I_S} \tag{2}$$

$$\phi(t) = \frac{4\alpha}{15} \frac{1}{I_S \lambda_X} \int_{-\infty}^{t} I_L(X, Y, c_0(t' - T), t') \underbrace{c_0 \, \mathrm{d}t'}_{\mathrm{d}z} \tag{3}$$

$$\Delta\phi(X, Y, T) = \frac{4\alpha}{15} \frac{c_0}{I_S \lambda_X} \int_{-\infty}^{\infty} I_L(X, Y, c_0(t - T), t) \, \mathrm{d}t \tag{4}$$

X, Y : transverse coordinate

T : time lag

$I_L = I_L(x, y, z, t)$: laser field

Single photon ellipticity and bunch effect

$$\begin{aligned}\Psi(X,Y,T) &\equiv |\delta|^2 = |\imath/2\Delta\phi(X,Y,T)|^2 \\ &= \frac{1}{4}\left(\frac{4\alpha}{15}\frac{c_0}{l_S\lambda_X}\right)^2\left[\int_{-\infty}^{\infty} I_L(X,Y,c_0(t-T),t)\,\mathrm{d}t\right]^2 \qquad (5)\end{aligned}$$

$$\begin{aligned}N_{\mathrm{flip}} &= N_X\int \Psi(x,y,t)f_{X,\,\mathrm{trans}}(x,y,\rho)f_{X,\,\mathrm{temp}}(t,\tau)\,\mathrm{d}x\,\mathrm{d}y\,\mathrm{d}t \qquad (6)\\ &\equiv N_X\epsilon\end{aligned}$$

Parameter overview for flipped photon count

Table 1 – Overview of beam parameters entering the calculation of the number of flipped photons per shot, cf. Eq. (6).

Quantity	Optical laser beam $I_L(x, y, z, t)$	XFEL probe beam $f_{X,trans}$, $f_{X,temp}$
pulse energy	$W_L = N_L \hbar\omega_L$	$W_X = N_X \hbar\omega_X$
wavelength	$\lambda_L = 2\pi c_0/\omega_L$	$\lambda_X = 2\pi c_0/\omega_X$
impact factor		ρ
time lag		τ

Parameter overview for flipped photon count

Table 1 – Overview of beam parameters entering the calculation of the number of flipped photons per shot, cf. Eq. (6), for Gaussian beams and pulses.

Quantity	Optical laser beam $I_L(x, y, z, t)$	XFEL probe beam $f_{X,trans}$, $f_{X,temp}$
pulse energy	$W_L = N_L \hbar\omega_L$	$W_X = N_X \hbar\omega_X$
wavelength	$\lambda_L = 2\pi c_0/\omega_L$	$\lambda_X = 2\pi c_0/\omega_X$
spot size	$w_L \approx \frac{\lambda_L}{\pi} 2F_\#$	w_X
pulse duration	τ_L	τ_X
impact factor	ρ	
time lag	τ	

Visual example 1: Spatial overlap

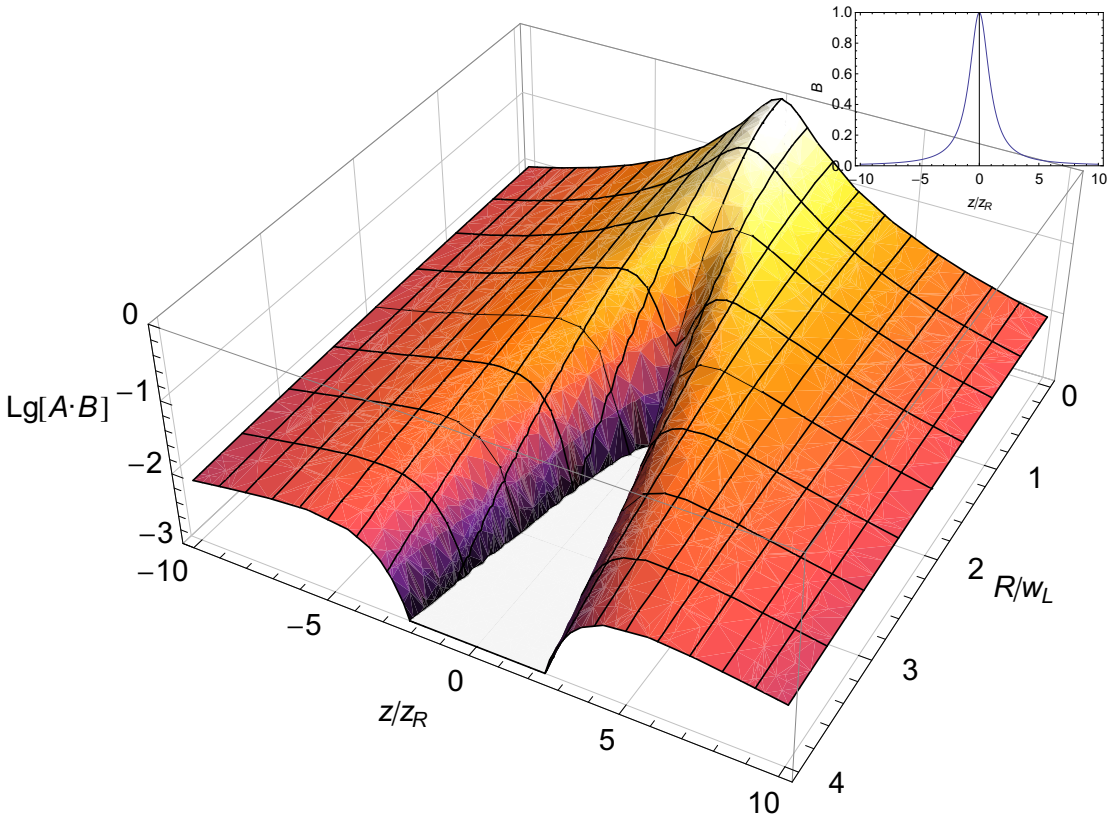

Figure 2 – Plot of transverse and longitudinal laser intensity dependence in log scale and in the range $10^{-3} \leq AB \leq 1$, as a function of z and R in units of z_R and w_L, respectively. The inset shows the Lorentz distribution (only longitudinal dependence) as a function of z in units of z_R in linear scale.

Visual example 2: Temporal overlap

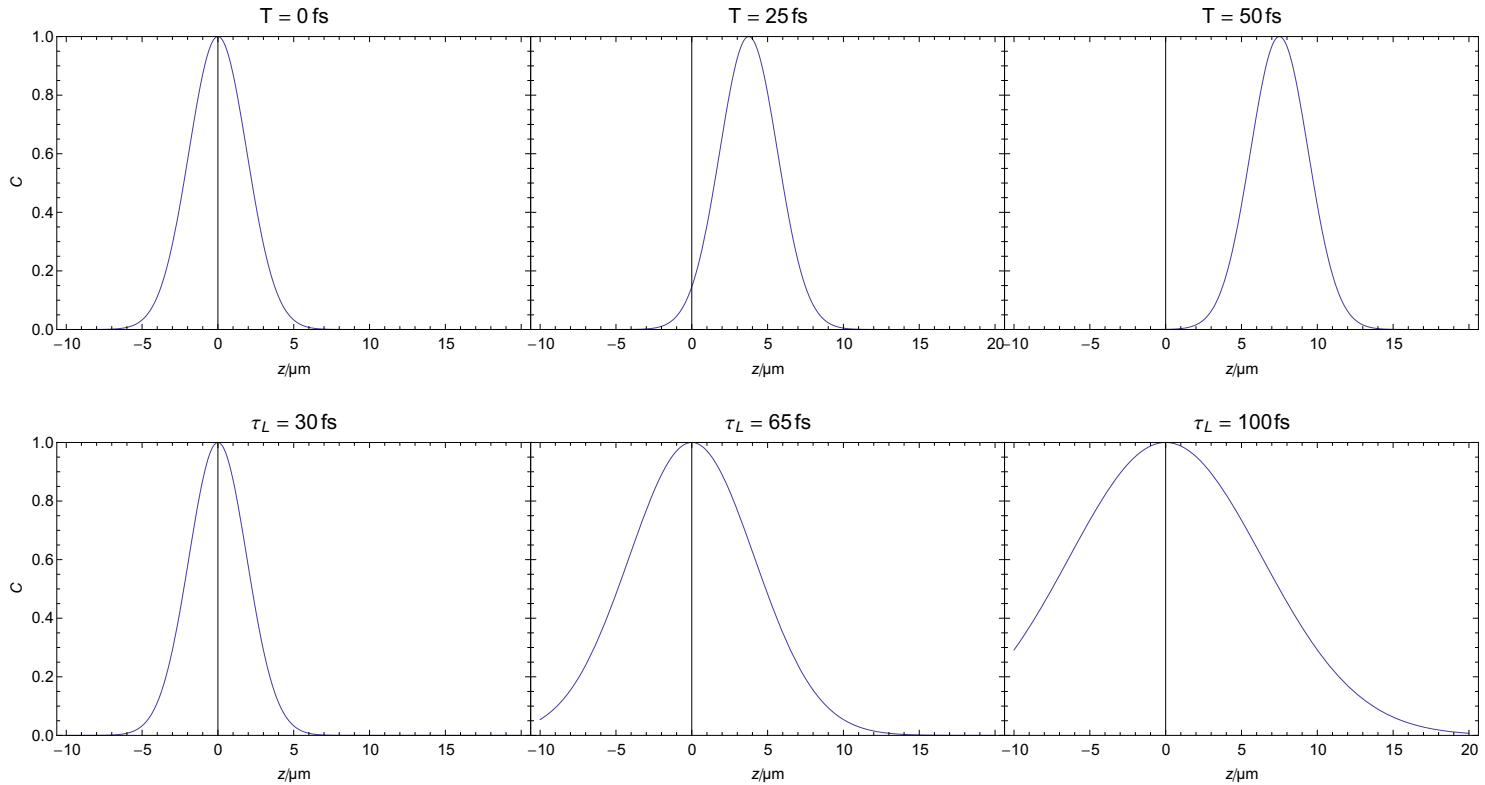

Figure 3 – Plots of temporal overlap regions for 2 parameter scans as function of z in microns. Top row: $\tau_L = 30\,\text{fs}$ constant and T varies. Bottom row: $T = 0\,\text{fs}$ constant and τ_L varies. Please note that $10\,\mu\text{m} \approx z_R$ for comparison with the previous plot.

Basic setup scheme

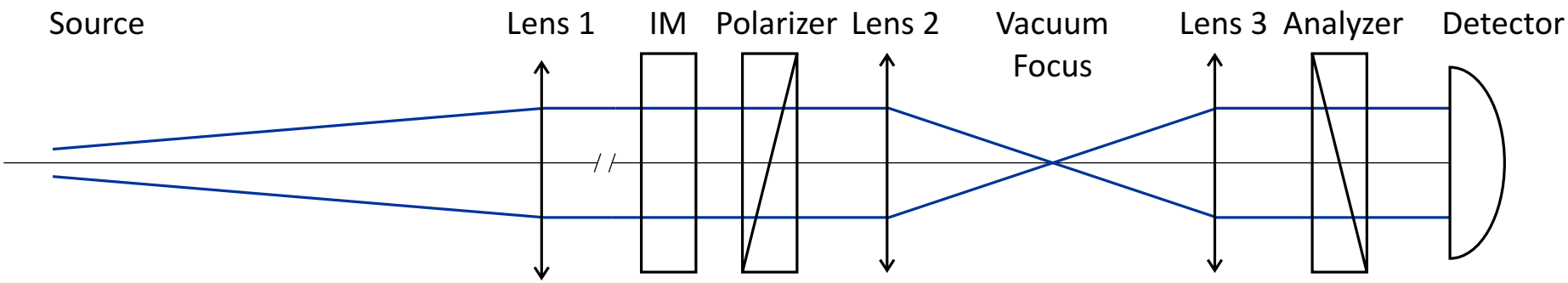

Figure 4 – Sketch of the X-ray beam path. X-rays are emitted from the source as a beam with some initial transverse width and divergence. A first CRL lens (Lens 1) is used to collimate the beam and maintain a reasonable beam width and flux. Once collimated, the beam passes through an intensity monitor (IM), recording shot-to-shot intensity fluctuations before the first channel-cut crystal (Polarizer) generates a linear polarization of high purity. The next stage consists of a symmetric set of CRLs (Lens 2 and 3) with relatively short focal lengths. They focus and re-collimate the beam, which finally passes the analyzer channel-cut crystal before it reaches the detector.

Detector signal

$$N_{\mathrm{det}} = N^{x}_{\mathrm{det}} + N^{y}_{\mathrm{det}} = N_{\mathrm{X}} \cdot T_{\mathrm{X}} \cdot (\beta_{\mathrm{pol}} + \epsilon)$$
$$= N_{\mathrm{X}} \cdot T_{\mathrm{X}} \cdot \beta_{\mathrm{pol}} \cdot \left(1 + \frac{\epsilon}{\beta_{\mathrm{pol}}}\right) , \tag{7}$$

We identify a background signal

$$N^{\mathrm{bg}}_{\mathrm{det}} \equiv N_{\mathrm{X}} \cdot T_{\mathrm{X}} \cdot \beta_{\mathrm{pol}} = \zeta N_{\mathrm{IM}} , \tag{8}$$

encoding the excellent but finite polarizer extinction β_{pol}, and

$$N^{\mathrm{QED}}_{\mathrm{det}} = N_{\mathrm{X}} \cdot T_{\mathrm{X}} \cdot \epsilon . \tag{9}$$

A key parameter governing the chances for detecting the QED effect is given by the ratio

$$\nu \equiv \frac{\epsilon}{\beta_{\mathrm{pol}}} . \tag{10}$$

DRESDEN concept

HZDR

Shot-to-shot-normalization and accumulation

We have to normalize somehow to N_X due to large (100%) fluctuations with help of N_{IM}:

$$R \equiv \frac{N_{det}}{\zeta N_{IM}} = 1 + \frac{N_{det}^{QED}}{N_{det}^{bg}} = 1 + \frac{\epsilon}{\beta_{pol}} = 1 + \nu \tag{11}$$

We also have to accumulate m shots to reduce the counting statistics error below the net signal count:

$$m \approx k^2 \frac{\beta_{pol}}{N_X T_X \epsilon^2} \propto \Delta\phi^{-4} \tag{12}$$

Interestingly, $\Delta\phi \propto W_L$, thus $m \propto W_L^{-4}$ and $T_{acq} = m/f_{rep,L} \propto W_L^{p-4}$ for $f_{rep,L} \propto W_L^{-p}$.
Also, further normalization of R with laser pulse energy is possible.

Observables summary

Table 2 – Summary of observables and relevant parameters governing the experiment.

Type	Variable	Explanation
1	N_{det}	primary observable
2	N_{IM}	reduces fluctuations due to $N_{\mathrm{det}} \propto N_{\mathrm{X}}$
3	W_{L}	reduces fluctuations due to $\epsilon \propto W_{\mathrm{L}}^2$
4	τ and ρ	pulse impact parameters caused by spatial and temporal jitter
5	τ_{L}, τ_{X}, w_{L}, w_{X}	basic beam parameters (2nd order moments)
6	I_{L}, $f_{\mathrm{X,trans}}$, $f_{\mathrm{X,temp}}$	full beam intensity distributions (higher order moments)
7	T_{X}, β_{pol}, ζ	instrumentation parameters

Essentially: Measure R in parameter space $(\rho, \tau, \ldots)$.

DRESDEN concept

HZDR

X-ray polarizer parameters

Table 3 – Properties of a Si800 6-bounce channel-cut crystal [6, 7], to be employed as X-ray polarizers.

Property	Value
incidence angle	$\theta = 45.000$
required photon energy	$E_\mathrm{X} = 12.914\,\mathrm{keV}$
extinction	$\beta_\mathrm{pol} \approx 6 \cdot 10^{-10}$
transmission	$T_\mathrm{pol} \approx 0.3$
angular acceptance	$\Delta\theta \lesssim 10\,\mu\mathrm{rad}$
spectral acceptance	$\frac{\Delta E_\mathrm{X}}{E_\mathrm{X}} \sim 10^{-4}$

X-ray source parameters

Table 4 – Overview of XFEL source parameters (from [8] and [9, Sec. 4.1.1]), assuming a Gaussian beam profile and a Gaussian pulse shape. The waist corresponds to a FWHM beam diameter of 50 µm.

Parameter	Value
photon energy	$E_X = 12.914\,\mathrm{keV}$
wavelength	$\lambda_X = 0.960\,\text{Å}$
photon number	$N_X = 5 \cdot 10^{12}$
pulse duration	$\tau_X = 20\,\mathrm{fs}$
source waist	$w_0 = 42.5\,\mu\mathrm{m}$
source divergence	$\Theta_0 = 1\,\mu\mathrm{rad}$
M-squared	$M^2 = 1.4$
pulse energy	$W_X = 10\,\mathrm{mJ}$
pulse peak power	$\hat{P}_{\mathrm{pulse}} = 0.5\,\mathrm{TW}$

Laser parameters

Table 5 – Overview of optical laser parameters. We assume a very short focusing device of $F_{\#} = f/2.5$.

Parameter	Value
wavelength	$\lambda = 800\,\mathrm{nm}$
pulse energy	$W_\mathrm{L} = 30\,\mathrm{J}$
pulse duration	$\tau_\mathrm{L} = 30\,\mathrm{fs}$
focus waist	$w_\mathrm{L} = 1.75\,\mu\mathrm{m}$
Rayleigh length	$z_\mathrm{R} = 12\,\mu\mathrm{m}$
peak power	$\hat{P}_\mathrm{L} = 1\,\mathrm{PW}$
peak intensity	$I_0 \approx 2 \cdot 10^{22}\,\mathrm{W/cm^2}$
	$\approx 4.4 \cdot 10^{-8} I_\mathrm{S}$

Results for ideal case: stable perfect overlap

$$\epsilon \approx 4 \cdot 10^{-12}$$

$$\nu \approx 0.00666\ldots$$

$$N_{\text{det}}^{\text{QED}} \approx 0.73 \text{ photons per shot}$$

$$N_{\text{det}}^{\text{bg}} \approx 110 \text{ photons per shot}$$

$$m(5\sigma) \approx 5 \cdot 10^{3} \text{ shots}$$

$$T_{\text{acq}}(5\sigma, 1\,\text{Hz}) \approx 1.5\,\text{hours}$$

Realistic jitter

Table 6 – Overview of jitter distribution parameters and sampling resolution of measurement devices.

	parameter τ	parameter ρ
sampling resolution	$\Delta_{\mathrm{BAM}} = 20\,\mathrm{fs}$	$\Delta_{\mathrm{FFM}} = 0.2\,\mu\mathrm{m}$
jitter rms	$\sigma_\tau = 50\,\mathrm{fs}$	$\sigma_\rho = 1.75\,\mu\mathrm{m} = w_{\mathrm{L}}$
initial jitter mean [1]	$\bar{\tau} = -17\,\mathrm{fs}$	$\bar{\rho} = -0.4\,\mu\mathrm{m}$
optimal jitter mean [2]	$\bar{\tau} = 35\,\mathrm{fs}$	$\bar{\rho} = 0.6\,\mu\mathrm{m}$

[1] not zero due to drifts
[2] not zero due to limited accuracy of alignment

DRESDEN concept

HZDR

Results of realistic case

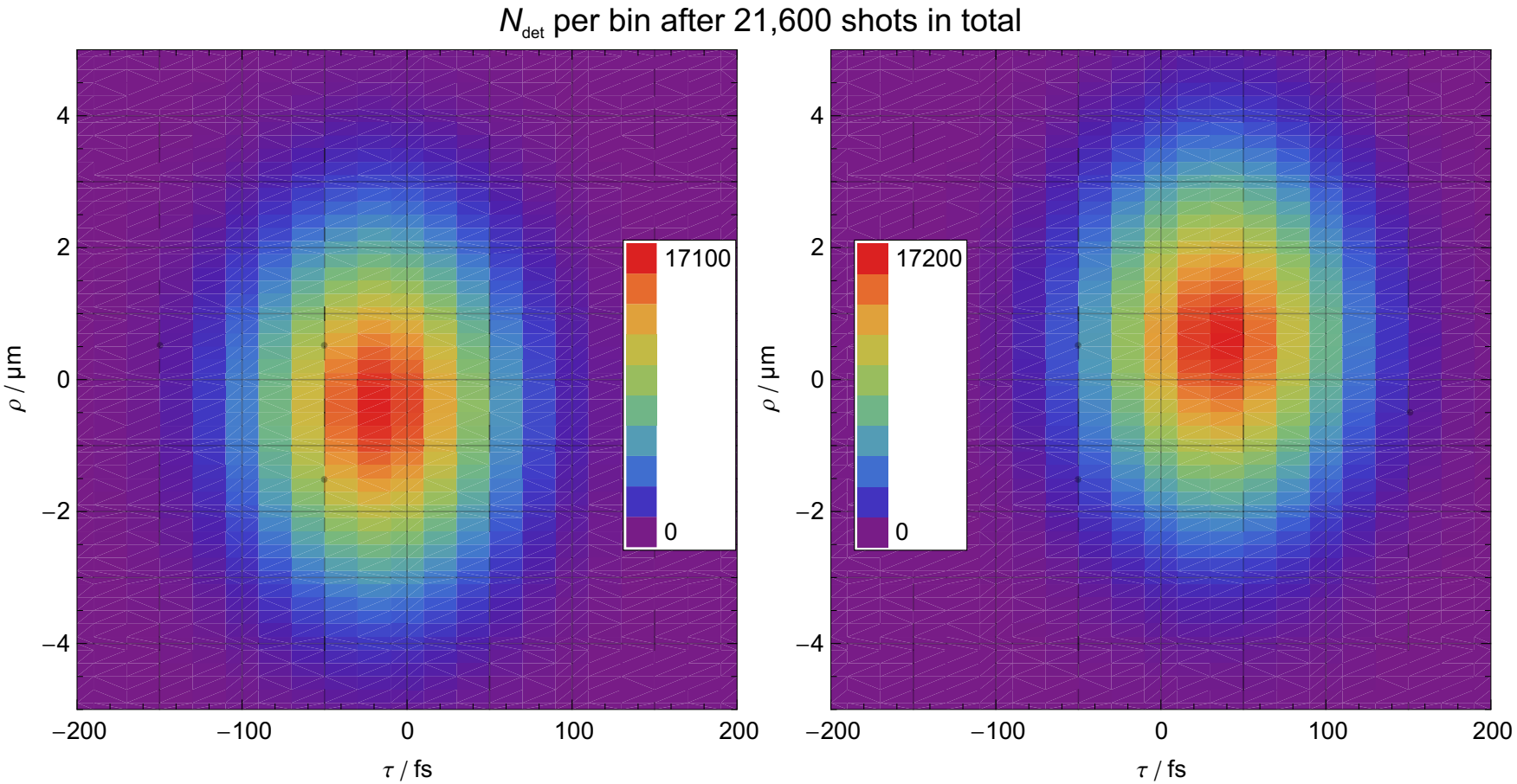

Figure 5 – Distribution of the number of detected photons, N_{det}, as a function of impact parameters ρ and τ. A total of 21,600 shots (6 hours) has been sorted into bins of size 20 fs × 0.2 µm. The distribution displayed is basically determined by the jitter distribution parameters of Table 6. Integration can yield the photon excess as $N_{det}^{QED} = N_{det} - \zeta N_{IM}$. Left: initial jitter conditions, $N_{det}^{QED} = 2611 \pm 1775$ photons; Right: optimized and re-adjusted mean values, $N_{det}^{QED} = 3803 \pm 1776$ photons.

DRESDEN concept

HZDR

Relative signal distribution

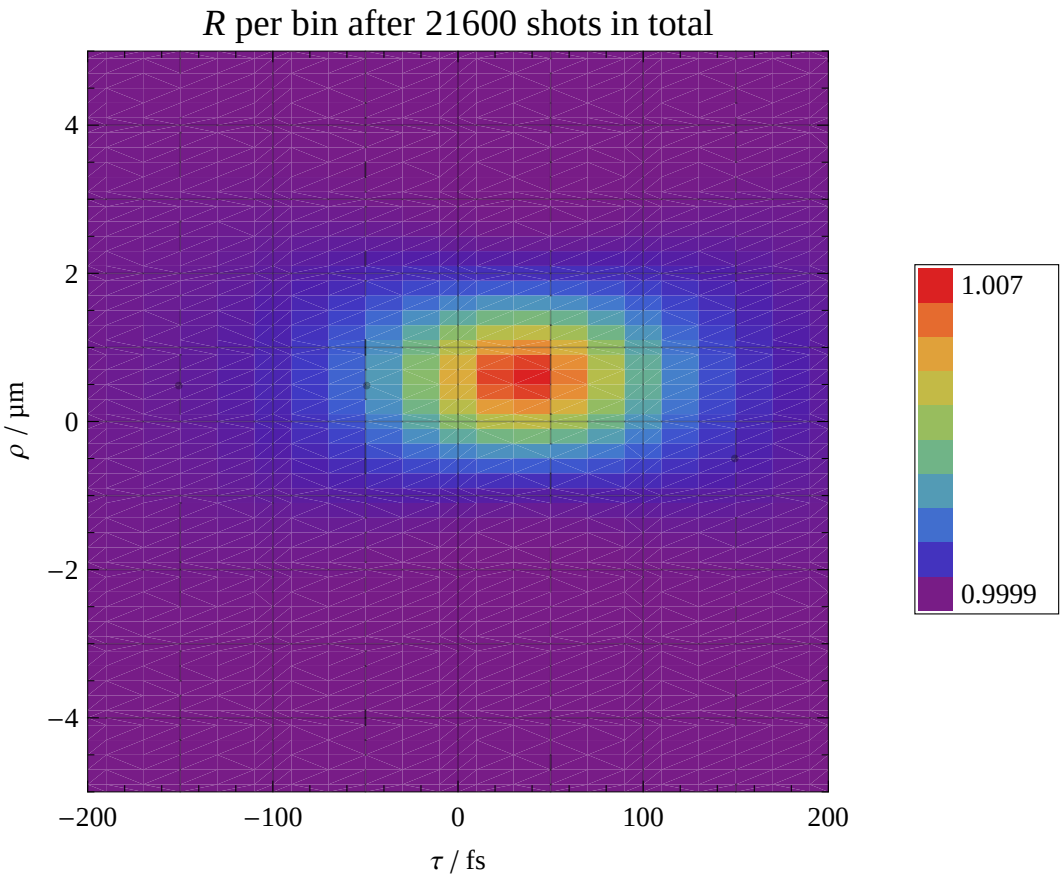

Figure 6 – Distribution of the ratio R as a function of impact parameters ρ and τ. (Shot number and bin size as in figure 5.) The distribution is independent of the jitter conditions. Its peak position is basically determined by the actual alignment, its shape by the individual pulse parameters (variables of types 5 and 6 in Tab. 2).

DRESDEN concept

HZDR

Synthetic example measurement results

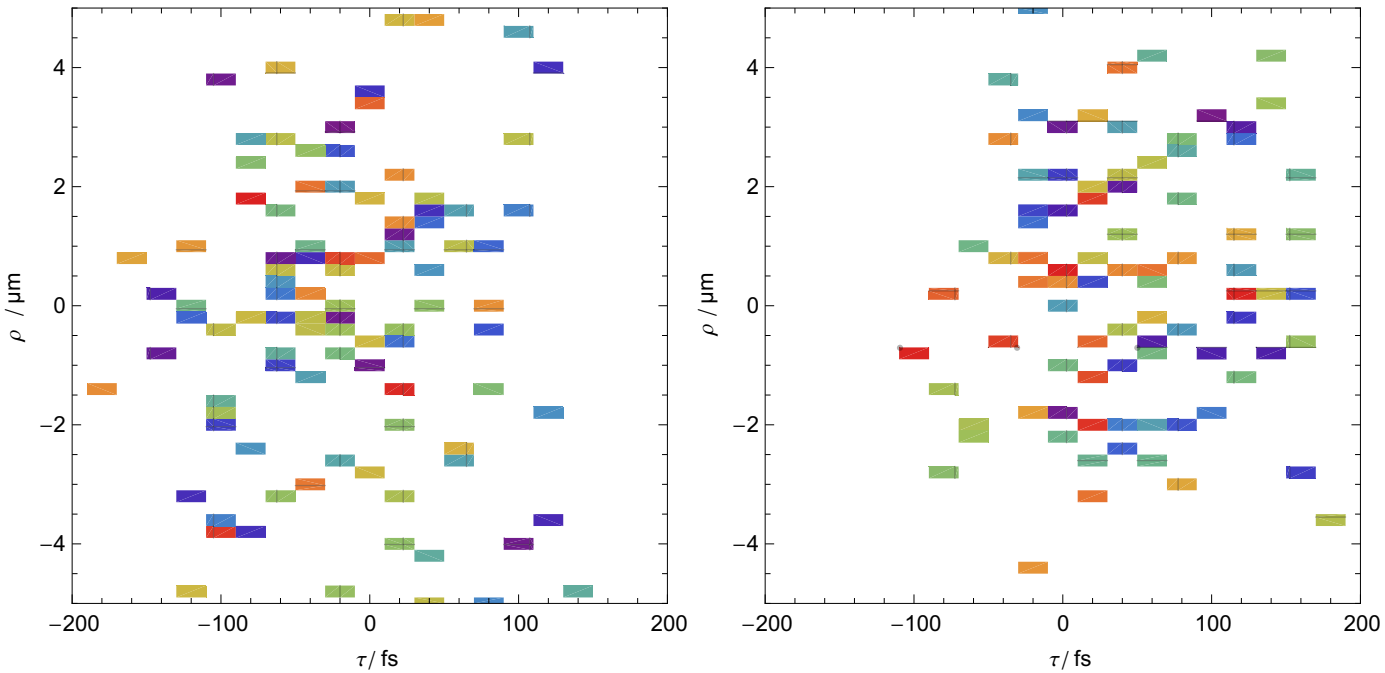

Figure 7 – Distribution of the ratio R as a function of impact parameters ρ and τ (bin size and color scale as before, cf. Fig. 6). The first slide represents a single run of 21,600 shots (6 hours), the second slide 100× more, i.e. 2.16×10^6 shots, improving the counting statistics by a factor of 10. Left: initial jitter conditions; Right: optimized and re-adjusted mean values.
The color range is the same as in Fig. 6 with all outliers beyond that range suppressed to avoid confusion. The peak position is again basically determined by the parameters of the jitter distribution, which may lead to a poor resolution of the peak position of R.

Synthetic example measurement results

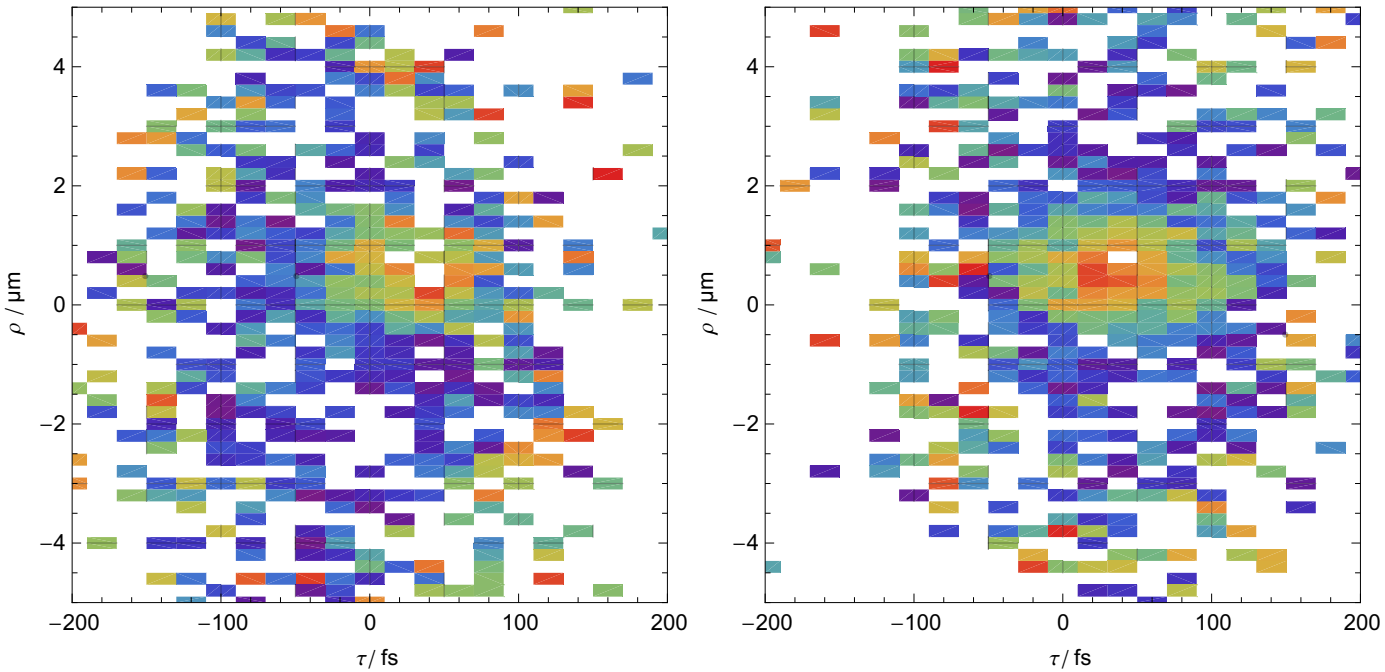

Figure 7 – Distribution of the ratio R as a function of impact parameters ρ and τ (bin size and color scale as before, cf. Fig. 6). The first slide represents a single run of 21,600 shots (6 hours), the second slide 100× more, i.e. 2.16×10^6 shots, improving the counting statistics by a factor of 10. Left: initial jitter conditions; Right: optimized and re-adjusted mean values.
The color range is the same as in Fig. 6 with all outliers beyond that range suppressed to avoid confusion. The peak position is again basically determined by the parameters of the jitter distribution, which may lead to a poor resolution of the peak position of R.

Summary (I)

- Refined previous model in simple manner to account for focused and pulsed beams
  - Strict forward scattering and solely polarization flip
  - Neglecting variations of refractive index for propagation
  - Recent work by Karbstein et. al. [5] fully(?) accounts for that
- Considered experimental setup and realization, observables, precautions, countermeasures, course of action
  - Crossed polarizers (polarimeter) plus 1:1-telescope
  - Rear end detector plus intensity monitor, further online monitors
- Conducted feasibility study based on current state-of-the-art facts and reasonably trustworthy predictions
  - European XFEL plus HIBEF
  - Channel-cut crystals plus compound refractive lenses

Summary (II)

- Results
  - Ideally few-hour measurement (30 J, 1 Hz), but depends on laser pulse energy (10 J, 5 Hz: 16 hours)
  - Jitter and drifts should be low
  - Alignment procedure should be accurate
- Outlook
  - Investigate Karbstein's work to measured only deflected photons
  - Study polarimetry with CRL telescope and XFEL beam

References (I)

[1] D. Hanneke, S. Fogwell, and G. Gabrielse. New Measurement of the Electron Magnetic Moment and the Fine Structure Constant. *Phys. Rev. Lett.*, 100:120801, 2008.

[2] Carl E. Carlson. The Proton Radius Puzzle. *Prog. Part. Nucl. Phys.*, 82:59–77, 2015.

[3] L. Meitner and H. Kösters. Über die Streuung kurzwelliger γ-Strahlen. *Z. Phys.*, 84:137, 1933.

[4] T. Heinzl, B. Liesfeld, K. U. Amthor, H. Schwoerer, R. Sauerbrey, and A. Wipf. On the observation of vacuum birefringence. *Opt. Comm.*, 267(2):318–321, November 2006.

[5] F. Karbstein, H. Gies, M. Reuter, and M. Zepf. Vacuum birefringence in strong inhomogeneous electromagnetic fields. 2015.

[6] B. Marx, I. Uschmann, S. Hoefer, R. Loezsch, O. Wehrhan, E. Foerster, M. Kaluza, T. Stoehlker, H. Gies, C. Detlefs, T. Roth, J. Hartwig, and G. G. Paulus. Determination of high-purity polarization state of x-rays. *Opt. Comm.*, 284(4):915–918, FEB 15 2011.

DRESDEN concept

HZDR

References (II)

[7] B. Marx, K. S. Schulze, I. Uschmann, T. Kaempfer, R. Loetzsch, O. Wehrhan, W. Wagner, C. Detlefs, T. Roth, J. Haertwig, E. Foerster, T. Stoehlker, and G. G. Paulus. High-precision x-ray polarimetry. *Phys. Rev. Lett.*, 110(25), JUN 21 2013.

[8] E.A. Schneidmiller and M.V. Yurkov. Photon beam properties at the european xfel. Technical Report XFEL.EU TR-2011-006, Deutsches Elektronen-Synchrotron (DESY), 2011.

[9] W. Decking and T. Limberg. European XFEL Post-TDR Description. Technical Note XFEL.EU TN-2013-004-01, European XFEL, Albert-Einstein-Ring 19, 22761 Hamburg, Germany, 2013.

to be continued

to be continued

around 2020

Backup slides

Overall setup

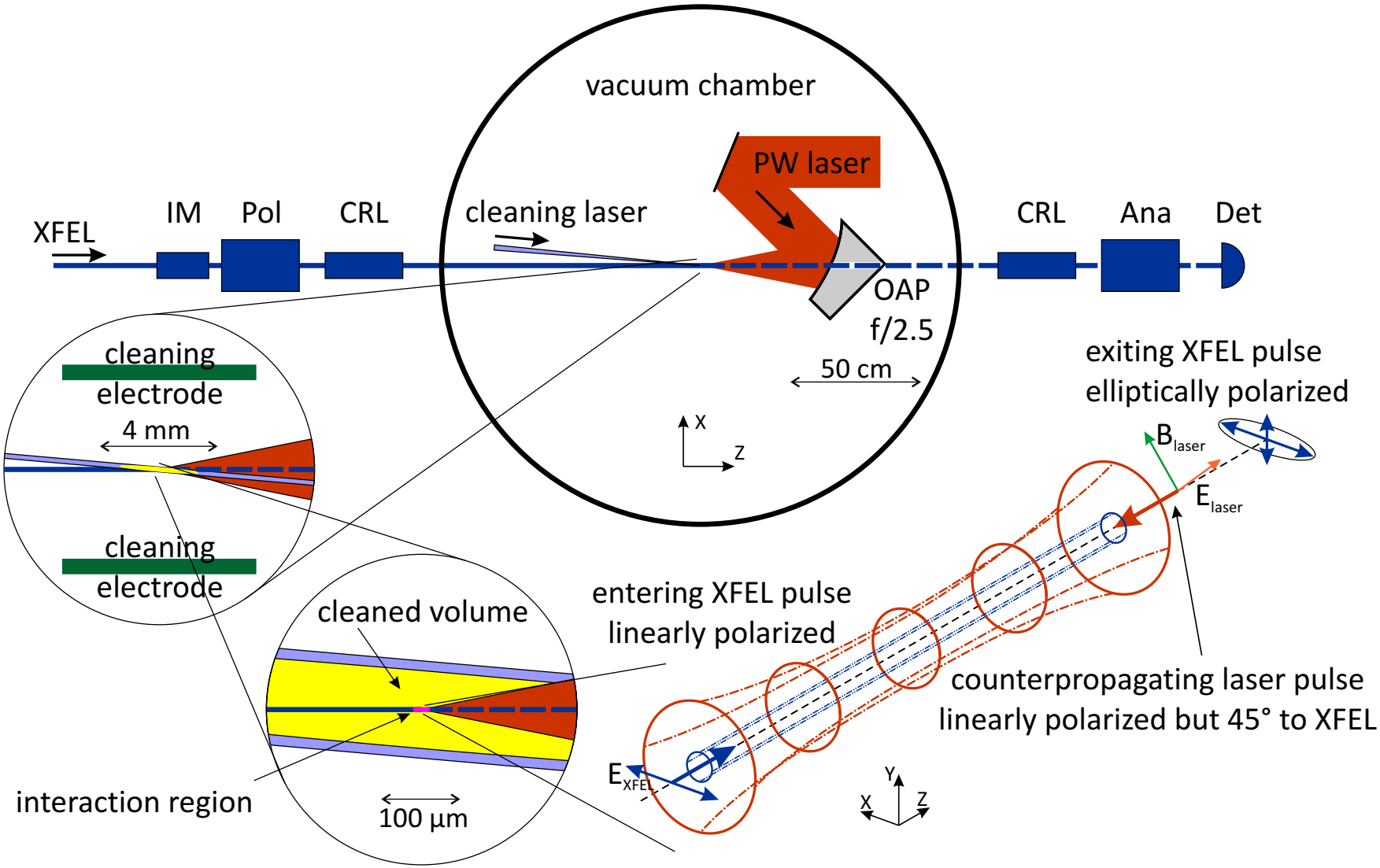

DRESDEN concept

HZDR

Gaussian beams (I)

$$I_{\mathrm{L}}(x, y, z, t) = I_0 \times A_{\mathrm{trans}}(x, y, z) \times A_{\mathrm{long}}(z) \times A_{\mathrm{temp}}(z, t) \tag{13}$$

$$A_{\mathrm{trans}}(x, y, z) = \exp\left[-2\frac{x^2 + y^2}{w(z)^2}\right] \tag{14}$$

$$A_{\mathrm{long}}(z) = \left[1 + \left(\frac{\lambda_{\mathrm{L}} z}{\pi w_{\mathrm{L}}^2}\right)^2\right]^{-1} \tag{15}$$

$$A_{\mathrm{temp}}(z, t) = \exp\left[-\ln 2\left(\frac{t + z/c_0}{0.5\tau_{\mathrm{L}}}\right)^2\right] \tag{16}$$

Gaussian beams (II)

$$z_R = \pi w_L^2 / \lambda_L \tag{17}$$

$$w(z) = w_L \sqrt{1 + \left(\frac{\lambda_L z}{\pi w_L^2} \right)^2} \tag{18}$$

$$I_0 = \frac{4\sqrt{\ln 2}}{\pi^{3/2}} \frac{W_L}{w_L^2 \tau_L} \simeq 0.60 \frac{W_L}{w_L^2 \tau_L} \tag{19}$$

$$w_L \approx \frac{\lambda_L}{\pi} 2F_\# \tag{20}$$

$$z_R \approx \frac{\lambda_L}{\pi} (2F_\#)^2 \tag{21}$$